Journal of Cellular Biochemistry 98:770–788 (2006)

ARTICLES

Quantifying Effects of Ligands on Androgen Receptor Nuclear Translocation, Intranuclear Dynamics, and Solubility

Marco Marcelli,[1,2,3] David L. Stenoien,[1] Adam T. Szafran,[1] Silvia Simeoni,[1] Irina U. Agoulnik,[1] Nancy L. Weigel,[1] Tim Moran,[6] Ivana Mikic,[5] Jeffrey H. Price,[4,5] and Michael A. Mancini[1]*

[1]Department of Molecular and Cellular Biology, Baylor College of Medicine, Houston, Texas
[2]Department of Medicine, Baylor College of Medicine, Houston, Texas
[3]Michael E. DeBakey VA Medical Center, Houston, Texas
[4]The Burnham Institute, San Diego, California
[5]Vala Sciences, Inc., San Diego, California
[6]Beckman Coulter, Inc., San Diego, California

Abstract Using manual and automated high throughput microscopy (HTM), ligand-dependent trafficking of green fluorescent protein-androgen receptor (GFP-AR) was analyzed in fixed and living cells to determine its spatial distribution, solubility, mobility, and co-activator interactions. Within minutes, addition of the agonist R1881 resulted translocation of GFP-AR from the cytoplasm to the nucleus, where it displayed a hyperspeckled pattern and extraction resistance in low expressing cells. AR antagonists (Casodex, hydroxyflutamide) also caused nuclear translocation, however, the antagonist-bound GFP-AR had a more diffuse nuclear distribution, distinct from the agonist-bound GFP-AR, and was completely soluble; overexpressed GFP-AR in treated cells was extraction resistant, independent of ligand type. To more dramatically show the different effects of ligand on AR distribution, we utilized an AR with a mutation in the DNA binding domain (ARC619Y) that forms distinct foci upon exposure to agonists but retains a diffuse nuclear distribution in the presence of antagonists. Live-cell imaging of this mutant demonstrated that cytoplasmic foci formation occurs immediately upon agonist but not antagonist addition. Fluorescence recovery after photobleaching (FRAP) revealed that agonist-bound GFP-AR exhibited reduced mobility relative to unliganded or antagonist-bound GFP-AR. Importantly, agonist-bound GFP-AR mobility was strongly affected by protein expression levels in transiently transfected cells, and displayed reduced mobility even in slightly overexpressing cells. Cyan fluorescent protein-AR (CFP-AR) and yellow fluorescent protein-CREB binding protein (YFP-CBP) in the presence of agonists and antagonists were used to demonstrate that CFP-AR specifically co-localizes with YFP-CBP in an agonist dependent manner. Dual FRAP experiments demonstrated that CBP mobility mirrored AR mobility only in the presence of agonist. HTM enabled simultaneous studies of the sub-cellular distribution of GFP-AR and ARC619Y in response to a range of concentrations of agonists and antagonists (ranging from 10^{-12} to 10^{-5}) in thousands of cells. These results further support the notion that ligand specific interactions rapidly affect receptor and co-factor organization, solubility, and molecular dynamics, and each can be aberrantly affected by mutation and overexpression. J. Cell. Biochem. 98: 770–788, 2006.

Key words: nuclear receptor; high throughput microscopy; GFP; FRAP; nuclear translocation

The androgen receptor (AR), a member of the steroid receptor superfamily, influences cell growth and differentiation by selectively regulating specific target gene expression in response to hormone [Lamb et al., 2001]. The mechanism through which AR and other nuclear receptors act as transcriptional regulators has been intensively scrutinized at the biochemical level leading to the development of a general model in which ligand binding induces conformational changes, loss of chaperones, dimerization, and nuclear translocation [Tsai

Grant sponsor: NIDDK; Grant number: DI-55622; Grant sponsor: NIDDK sponsored Center for Reproductive Biology; Grant number: U54 HD-96-008; Grant sponsor: Prostate Spore; Grant number: CA58204.

*Correspondence to: Michael A. Mancini, Department of Molecular and Cellular Biology, Baylor College of Medicine, Houston, TX 77030. E-mail: mancini@bcm.tmc.edu

Received 10 March 2005; Accepted 11 March 2005
DOI 10.1002/jcb.20593

and O'Malley, 1994; Mangelsdorf et al., 1995]. While agonist induces nuclear localization of AR [Jenster et al., 1993], many other steroid receptors including the estrogen receptor (ER) [King and Greene, 1984; Welshons et al., 1988; Htun et al., 1999; Stenoien et al., 2000] are nuclear regardless of their ligand bound state indicating that mechanisms exist within the nucleus to prevent transcription by unliganded receptor.

As AR plays an important role in prostate cell proliferation and differentiation, manipulation of AR function is a primary treatment for patients diagnosed with prostate cancer. Pure antiandrogens such as hydroxyflutamide (OHF) and Casodex (Cas) act as competitive inhibitors and are used in association with chemical castration to treat patients with advanced prostate cancer (Reviewed in [Reid et al., 1999]). After a median response of 18–24 months these androgen ablative therapies fail and patients develop androgen-independent (AI) disease. AI prostate cancer is incurable and leads to death of approximately 30,000 Americans every year [Jemal et al., 2004]. Active research is trying to explain the molecular mechanisms of prostate cancer transition to AI disease, and leading hypotheses are that the requirement for AR function is bypassed by the cancer cell or that alternative pathways or AR mutations create novel intracellular mechanisms leading to AR activation in spite of the androgen-depleted endocrine milieu that is present in these individuals [Feldman and Feldman, 2001]. Studies on AR gene mutations associated with prostate cancer have found an increased incidence of mutations in patients with advanced disease, especially following anti-androgen therapy [Marcelli et al., 2000]. One such mutation studied by our group, C619Y [Nazareth et al., 1999], forms intranuclear inclusions in response to hormone addition, suggesting that alteration of AR function may play a role in the progression of the disease. For this reason it is important to fully understand normal AR function and the effect that ligands have upon the complicated relationship between transactivator function and sub-cellular organization.

Live-cell imaging studies of GFP-tagged steroid receptors have been very useful in elucidating the dynamic nature of this class of proteins [McNally et al., 2000]. Changes in the intranuclear distribution of GFP-ER and recruitment of co-activators occur within minutes of exposure [Htun et al., 1999; Stenoien et al., 2000]. Similar rapid dynamics have also been observed for other steroid receptors including glucocorticoid receptor, mineralocorticoid receptor [Fejes-Toth et al., 1998], and AR [Georget et al., 1997; Stenoien et al., 1999; Tyagi et al., 2000; Tomura et al., 2001; Saitoh et al., 2002]. In the case of GFP-AR, both agonists and antagonists can promote nuclear translocation, however, only agonists cause GFP-AR to form discrete intranuclear foci that co-localize with co-activators [Saitoh et al., 2002].

Based on previous investigations that show a tight correlation between steroid receptor function, intranuclear targeting, nuclear matrix association, and co-regulator interactions, we utilized a live and fixed cell approach to study the effects of ligand binding on green fluorescent protein-AR (GFP-AR) dynamics. Consistent with our previous results with ER [Stenoien et al., 2000, 2001b], the agonist-bound GFP-AR adopts a defined hyperspeckled subnuclear distribution that is clearly correlated with both decreased solubility and mobility. We also tested the effects of ligand on co-activator recruitment and found that only agonist addition results in the recruitment of YFP-CBP to CFP-AR speckles. Finally, the details of AR nuclear translocation were studied with the aid of HTM, and we found that while agonist activity rapidly induced quantifiable nuclear organization that is consistent with transcription function, antagonist consistently resulted in diffuse intranuclear organization, consistent with lack of transcriptional activity of wild type AR. These results indicate that agonist binding specifically initiates a complex cascade of events that include nuclear translocation, hyperspeckle formation, and co-activator recruitment.

MATERIALS AND METHODS

Reagents

All chemicals were obtained from Sigma-Aldrich (St. Louis, MO) unless stated otherwise. Casodex (ICI 176,334) was obtained from Dr. B. Vose, ICI Pharmaceutical Macclesfeld, UK. Methyltrienolone (R1881) from NEN Life Science Products (Boston, MA).

Mammalian Expression Plasmids

CFP-AR was made by swapping the Age-1/Bgl II fragment containing CFP from pECFP-C1

into GFP-AR [Stenoien et al., 1998] digested with the same two enzymes. YFP-CBP was described previously [Stenoien et al., 2001a].

Cell-Culture and Labeling

HeLa cells were maintained in Opti-MEM I media (Life Technologies, Inc., Gaithersburg, MD) containing 4% FBS (Life Technologies, Inc.). Twenty-four hours before transfection, cells were plated onto poly-D-lysine-coated coverslips in 35-mm wells at a concentration of 10^5 cells per well in media containing charcoal stripped FBS. Transient expression of plasmids was accomplished using Fugene (Roche Diagnostics, Indianapolis, IN).

Live Microscopy and FRAP

Cells were grown on 40-mm cover slips in 60-mm plates and transfected with 2.5 μg of each test plasmid, allowed to recover for 4–24 h and then were transferred to a live-cell chamber (Bioptechs, Inc., Butler, PA) and maintained in DMEM with 5 % stripped FBS at 37°C. This medium was recirculated using a peristaltic pump to which ligand was added. Live microscopy was performed using a Deltavision deconvolution microscope (Applied Precision, Issaquah, WA) with images acquired before and at time intervals following ligand addition. A Z-series of focal planes were digitally imaged and deconvolved with the DeltaVision constrained iterative algorithm to generate higher-resolution images.

For live cell half-FRAP experiments, HeLa cells grown on 23-mm glass bottom Delta T dishes (Bioptechs), transfected with 0.4 μg of each test plasmid plus 0.8 μg of carrier DNA using Transfectin (BioRad), and allowed to recover for 24 h before being placed onto a LSM 510 confocal microscope (Carl Zeiss, Thornwood, NY) equipped with a 63X (NA 1.4) objective. Cells were maintained at 37°C using a Bioptechs Delta Controller and fresh media containing the appropriate ligand was cycled over the cells. A single Z-section was imaged before and at time intervals following the bleach. The bleach was performed using the laser set 488 nm for GFP at maximum power for 4 iterations (~1 s). For dual FRAP experiments, both GFP and CFP tagged proteins were bleached with the 458 nm laser line and simultaneous images corresponding to the CFP and YFP fluorescence were obtained. Fluorescent intensities of regions of interest were determined using LSM software and data was exported to Excel (Microsoft, Inc.) for analysis. LSM images were exported as TIF files and final figures were generated using Adobe Photoshop and Illustrator.

High Throughput Microscopy

Experiments were performed using HeLa cells obtained from ATCC (Manassas, VA) maintained in phenol red-free, Opti-MEM I medium (Life Technologies, Inc., Gaithersburg, MD) containing 4% FBS (Life Technologies, Inc.) and penicillin/streptomycin.

Twenty-four hours before transfection, cells were plated onto 10-cm plastic dishes in medium containing charcoal stripped FBS. Transient expression of GFP-AR and GFP-AR619 [Nazareth et al., 1999] was performed using 2.5 μg expression plasmid and 7.5 μg carrier DNA (BlueScript, Stratagene, San Diego, CA) using Fugene. After overnight incubation, DNA was removed, and replaced with fresh medium for 24 h. Cells were then trypsinized and replated at 5,000 cells per well in NUNC-CC2 tissue culture treated 96-MicroWell optical glass bottom plates (Nalge Nunc, NY) and incubated overnight. Cells were then exposed for 2 h to vehicle at 11 different ligand concentrations (Table I) prior to washing in PBS and fixation for 30 min at RT in 4% formaldehyde prepared in CSK buffer (80 mM potassium PIPES, pH 6.8, 5 mM EGTA, 2 mM $MgCl_2$). Cells were then placed in 0.4% formaldehyde in CSK until image analysis. Image analysis was preceded by washing in PBS, aspirating the washed solution, adding 150 μL Hoechst antifade solution, and adding 150 μl of prolong antifade (Molecular Probes, Eugene, OR) containing 1 μg/ml DAPI. Ligands consisting of agonist (R1881) and antagonists (Casodex, Cas; hydroxyflutamide, OHF; and estradiol, E2) were added to wells for 2 h to achieve final concentrations as outlined in Table I. The well plate was organized in a way that wild type or mutant GFP-tagged androgen receptors were in triplicate or quadruplicate, respectively.

The Beckman/Q3DM IC-100 high throughput microscope (HTM) system was used to automate fluorescent image acquisition and analysis of the AR Nuclear Translocation and Foci Formation (NTFF) assay. The primary system components consist of a standard fluorescent inverted microscope (Nikon TE-2000, Melville, NY); a Pentium 4/Xenon workstation (Compaq,

TABLE I. 96-Well Plate Lay-out for HTM

R1881											
No horn	10^{-7} M	5×10^{-8} M	10^{-8} M	5×10^{-9} M	10^{-9} M	5×10^{-10} M	10^{-10} M	5×10^{-11} M	10^{-11} M	5×10^{-12} M	10^{-12} M
WT	WT	WT	WT	WT	WT	WT	WT	WT	WT	WT	WT
619	619	619	619	619	619	619	619	619	619	619	619
Z										Z	
CASODEX											
No horn	10^{-5} M	5×10^{-6} M	10^{-6} M	5×10^{-7} M	10^{-7} M	5×10^{-8} M	10^{-8} M	5×10^{-9} M	10^{-9} M	5×10^{-10} M	10^{-10} M
WT	WT	WT	WT	WT	WT	WT	WT	WT	WT	WT	WT
619	619	619	619	619	619	619	619	619	619	619	619
Z										Z	
Flutamide											
No Horn	10^{-5} M	5×10^{-6} M	10^{-6} M	5×10^{-7} M	10^{-7} M	5×10^{-8} M	10^{-8} M	5×10^{-9} M	10^{-9} M	5×10^{-10} M	10^{-10} M
WT	WT	WT	WT	WT	WT	WT	WT	WT	WT	WT	WT
619	619	619	619	619	619	619	619	619	619	619	619
Z											
Estradlol											
No horn	10^{-6} M	5×10^{-7} M	10^{-7} M	5×10^{-8} M	10^{-8} M	5×10^{-9} M	10^{-9} M	5×10^{-10} M	10^{-10} M	5×10^{-11} M	10^{-11} M
WT	WT	WT	WT	WT	WT	WT	WT	WT	WT	WT	WT
619	619	619	619	619	619	619	619	619	619	619	619
Z											

Four Ligands (R1881, Casodex, Hydroxyflutamide and Estradiol) were used in a dilution serre, as described; Ethanol was used as a vehicle (Veh) control. WT refers to wild type AR and 619 refers to the C619Y AR mutation. Both receptors were GFP-tagged on its N-terminus.

Houston, TX); a Beckman/Q3DM control system, which houses the electronic components; and Beckman/Q3DM's CytoShop^{TM} software, which controls the system for acquisition before analyzing the acquired images. The objective used in the scan was a Nikon S. Fluor 40×0.95 NA. The spatially and temporally stabilized fluorescent light source is a proprietary Beckman/Q3DM design, which uses a 100 watt Osram HBO 103 W/2 mercury arc lamp (Osram Sylvania, Danvers, MA) as its light source and connects to the microscope at the Nikon epi-fluorescent attachment. A standard Chroma (Brattleboro, VT) 82000 triple band filter set was used for fluorescent imaging. 12-bit images were acquired on a Hamamatsu (Bridgewater, NJ) ORCA-ER scientific grade camera with 1×1 binning ($1{,}344 \times 1{,}024$ pixels; 6.45 μm^2 pixel size).

The system was used to scan multiple fields from well to well and to acquire and analyze each of the cells in the images. Algorithms were generated to calculate cytosol-to-nucleus translocation [Fractional Localized Intensity in the Nucleus (FLIN)], Nuclear VARiation of fluorescence intensity [NVAR], and formation of foci/vesicles [Fractional Localized Intensity in the Vesicle (FLIVSUM)] in response to the various ligands. EC50 were calculated. Nuclear and foci area masks were generated by applying a nonlinear least-squares optimized image filter to create marked object-background contrast, followed by automatic histogram-based thresholding. Effects due to background fluorescence were corrected by estimating and subtracting the mean background image intensity, which is dynamically determined on a per-image basis. The correlated channel mask was computed as an intersection between the threshold correlated channel image (the threshold level is dynamically computed using a proprietary background level estimation method), a Voroni tessellation polygon, and a circle of user-defined radius from the nuclear centroid. Threshold gates were applied to each of the data sets to first extract a sub-population of single cell objects, and further extract a sub-population of single cell objects that were identified as transfected, then further gated to measure only the bottom $\sim$10% of the GFP-positive cells to avoid overexpression artefacts. Transfected cell sub-populations were used to generate well-plate maps (data not shown) and dose-response curves (Figs. 4 and 5). Each point of the dose-response

curve was expressed as mean ± SD of the four time points.

AR Transcription Assay

AR transcription assays were performed as reported in Agoulnik et al. (2003). Briefly, HeLa cells were plated in 6-well plates at 180,000 cells per well in DMEM media supplemented with 5% charcoal stripped FBS. The next day cells were transfected with 400 ng of GRE_2-E1b-Luc reporter, 30 ng of pCR3.1-β-Galactosidase, 5 ng of either pCFP-AR or pCR3.1 AR, and 400 ng of either pYFP-CBP or vector pYFP, using poly-lysine-coupled adenovirus for 2 h in serum-free Dulbecco's modified Eagle's medium (Invitrogen) [1]. Media with 10% charcoal-stripped FBS was added to give a final concentration of 5% and cells were then treated with either 3 nM of androgen agonist R1881 or left untreated. Twenty-four hours later, cells were rinsed with PBS (Invitrogen), lysed and assayed for luciferase and β-Galactosidase activity as described in [1]. Background activity (activity without hormone) was subtracted from the activity in the presence of the agonist. Relative luciferase units (RLU) were normalized for β-Galactosidase activity, the values averaged and standard deviation calculated. Each point was done in triplicate and experiments were repeated three times.

RESULTS

AR Distribution in Response to Agonist and Antagonists

The addition of agonist results in the nuclear translocation of AR [Jenster et al., 1993]. To determine the dynamics of nuclear translocation, green fluorescent protein-tagged ARs (GFP-AR) have been used to analyze AR distribution in living cells [Georget et al., 1997; Stenoien et al., 1999; Tyagi et al., 2000; Tomura et al., 2001; Saitoh et al., 2002]. In the present study, we use both GFP-AR and a cyan fluorescent protein-AR (CFP-AR) that also allows for dual examination with proteins tagged with yellow fluorescent protein (YFP). Both GFP-AR and CFP-AR are transcriptionally active, however, to a lesser extent (~50%) than untagged AR (data not shown, and [Tomura et al., 2001]). In most cells analyzed, R1881 addition (10^{-8} M) caused GFP-AR to accumulate in the nucleus within 10 min; by 30 min, translocation was complete (Fig. 1). Throughout this study, we specifically examined GFP-AR positive cells that are just above the detection level of our instrumentation (e.g., overexpressors are excluded; see below). These data are in agreement with time series studies using fixed cells and untagged AR (data not shown and [Jenster et al., 1993]). In addition to causing nuclear

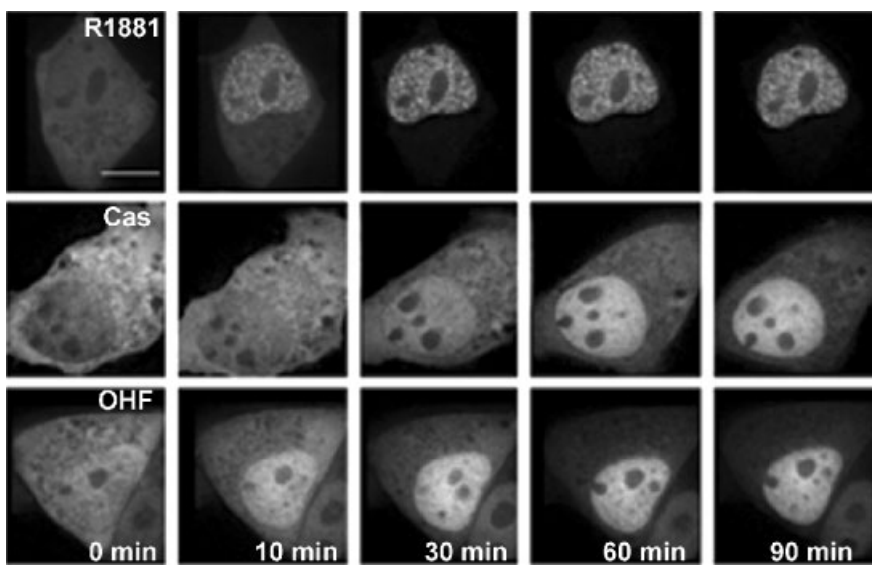

Fig. 1. Live microscopy of GFP-AR. HeLa cells were transiently transfected with GFP-AR and were imaged live during the addition of R1881 (5×10^{-9} M), Casodex (10^{-6} M; Cas), or hydroxyflutamide (OHF; 10^{-6} M). R1881 induces a rapid cellular reorganization of GFP-AR that includes nuclear translocation and hyperspeckled foci formation. Cas and OHF induce nuclear translocation of GFP-AR, albeit at a slower rate, but with no intranuclear hyperspeckling.

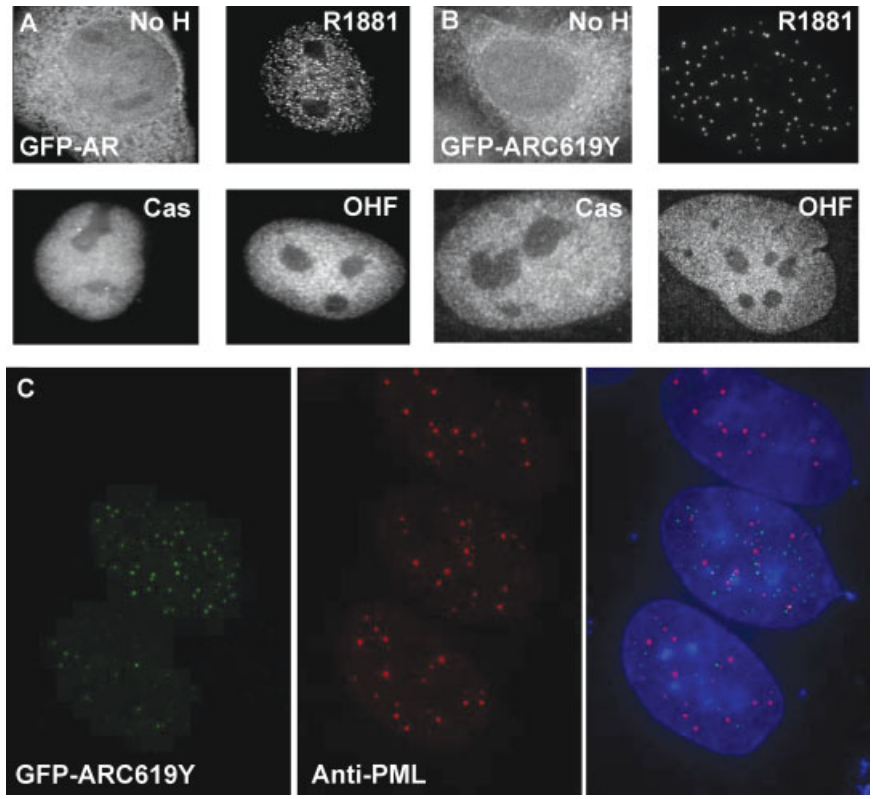

Fig. 2. Higher resolution images of GFP-AR. HeLa cells transiently transfected with GFP-AR (**A**) or GFP-ARC619Y (**B**) were incubated for 1 h with vehicle (ethanol), R1881 (5×10^{-9} M), Cas (10^{-6} M), and OHF (10^{-6} M). R1881 induces a nuclear hyperspeckled distribution of the wild type receptor and larger foci of the mutant receptor. The antagonists Cas and OHF induce nuclear translocation but fail to induce hyperspeckle formation. To determine if the foci formed by GFP-ARC619Y are related to PML bodies, a co-localization experiment was performed with GFP-ARC619Y and an antibody recognizing PML bodies (**C**). In the merged image (with DAPI-stained DNA blue), no overlap was observed in the two fluorescent patterns suggesting that GFP-ARC619Y foci are not PML bodies.

translocation, agonist also results in the progressive reorganization of GFP-AR into distinct intranuclear foci that are more evident at higher magnification (Fig. 2A).

We next analyzed the effects of the antagonists Cas 10^{-6} M (Fig. 1B) and OHF 10^{-6} M (Fig. 1C) on GFP-AR distribution. Live microscopic imaging revealed that both Cas and OHF promote slower nuclear translocation of GFP-AR compared to R1881. In the presence of Cas, GFP-AR approached a predominant nuclear distribution only after 60 min of treatment, and still exhibited substantial cytoplasmic localization even after 90 min. Similarly, OHF induced a partial nuclear translocation in 30 min, and translocation remained incomplete after 90 min. In agreement with results reported by others [Tyagi et al., 2000; Tomura et al., 2001], both Cas and OHF failed to induce a hyperspeckled intranuclear distribution of GFP-AR (Fig. 2A).

To further investigate the differential localization of GFP-AR caused by agonists and antagonists, we utilized an AR containing a point mutation in the DNA binding domain (11) that inactivates the transcriptional ability of the receptor. As shown previously, the localization of the unliganded mutant was indistinguishable from that of the wild type receptor, however, following treatment with agonist, the mutant receptor formed very distinct intranuclear foci that sequestered SRC-1 (steroid receptor co-activator-1) [Nazareth et al., 1999]. Fixed cell analysis of GFP-ARC619Y showed that the unliganded receptor had a diffuse and predominantly cytoplasmic distribution (Fig. 2B). Following treatment with R1881 (10^{-8}; 1 h), GFP-ARC619Y localized to discrete foci that were larger and fewer in number than those formed by GFP-AR. In the presence of Cas (10^{-6}; Fig. 2C) or OHF (10^{-6}; Fig. 2D), GFP-ARC619Y had a diffuse intranuclear distribu-

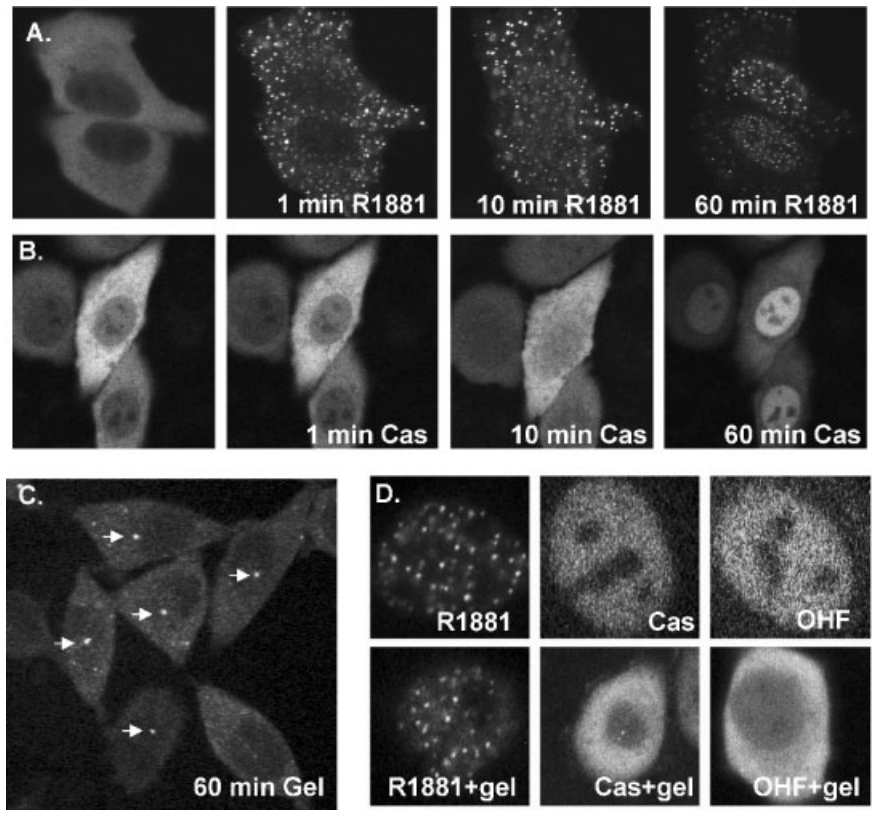

Fig. 3. Live-cell imaging of GFP-ARC619Y. HeLa cells were transiently transfected with GFP-ARC619Y and visualized live during the addition of R1881 ($5x10^{-9}$ M) or Cas (10^{-6} M). Addition of R1881 induces a rapid appearance of cytoplasmic foci that gradually localize in the nucleus over time (**A**). Cas induces nuclear translocation of GFP-ARC619Y with no evidence of foci formation (**B**). Treatment of cells with geldanamycin (1 μg/ml; 1h) resulted in some cells with cytoplasmic foci, while many other cells showed accumulations of GFP-AR at the centrosome (arrows; co-localization with anti-centrosome antibody not shown) (**C**). To determine the effects of geldanamycin on ligand-bound mutant AR, cells were incubated with hormone alone for 1 h (**D** top panels) or incubated with hormone for 1 h followed by a 1 h incubation with hormone + geldanamycin. In the presence of R1881, geldanamycin had no effect on the nuclear localization of GFP-ARC619Y. Interestingly, geldanamycin reversed the nuclear localization of antagonist-bound GFP-ARC619Y (**D**, lower panels).

tion that was clearly distinct from the agonist bound receptor. Since PML bodies have recently been implicated as playing a role in sequestering steroid receptor co-activators [Rivera et al., 2003], co-localization experiments were performed with an anti-PML antibody. As shown in 2C, no co-localization was observed with the GFP-C619Y foci and PML bodies.

Live-cell imaging of cells transfected with GFP-ARC619Y revealed that R1881 caused the mutant receptor to form cytoplasmic foci within ~1 min of hormone exposure (Fig. 3A). Over the course of 1 h there was a gradual shift of GFP-ARC619Y foci in the nucleus. The intranuclear foci gradually became larger and brighter as time progresses suggesting GFP-ARC619Y translocated into the nucleus as individual subunits rather than as intact clusters of protein. No cytoplasmic foci were observed when Cas (Fig. 3B) or OHF (data not shown) was added. Instead, a gradual shift in the diffuse cytoplasmic pool to a diffuse nuclear pool was observed. These data suggests that antagonists induce a different conformation of ARC619Y, both in the nucleus and in the cytoplasm immediately after hormone exposure.

One possibility for the differential localization caused by antagonists may be impaired dissociation of molecular chaperones that prevents ARC619Y from forming inclusions. In support of this, Georget et al., presented evidence that antagonist-bound ARs remain associated with Hsp90. To test this in our system, live cells were treated with geldanamycin, which disrupts both hsp90 function and normal steroid receptor trafficking [Czar et al., 1997]. Treatment of cells with geldanamycin (1 μg/ml; 1h) resulted in some cells with

cytoplasmic foci, while many other cells showed accumulations of GFP-C619YAR at the centrosome/aggresome (Fig. 3C; co-localization with anti-centrosome antibody not shown) [Kopito, 2000]. Treatment with geldanamycin followed by addition of agonist was associated with lack of nuclear translocation (data not shown). To determine the effects of geldanamycin on ligand-bound receptors, cells were incubated with hormone alone for 1 h (Fig. 3D, top panels) or incubated with hormone for 1 h followed by a 1 h incubation with hormone + geldanamycin. In the presence of R1881, geldanamycin had no effect on the nuclear localization of GFP-ARC619Y. Interestingly, geldanamycin reversed the nuclear localization of antagonist-bound GFP-ARC619Y, suggesting antagonists do not fully release Hsp90 even if translocated to the nucleus, and as a result can reverse nuclear targeting (Fig. 3D, lower panels).

AR and C619Y Intracellular Compartmentation Using HTM

Fully automated (or image cytometry) can acquire and analyze fluorescent images of large numbers of cells from thousands of microscopic fields of view per hour. Transient transfection of GFP-fused AR-WT and ARC619Y into HeLa were examined for nuclear translocation [Fractional Localized Intensity in the Nucleus (FLIN)] and formation of hyperspeckled intranuclear foci based upon the Nuclear VARiation of fluorescence intensity [NVAR] in response to an 11-point dose response of an agonist (R1881), antagonists (Cas, or E2). E2 is an AR antagonist, except at high concentration, where it is a weak agonist, for example, at $\sim 10^{-6}$ M. All ligand exposures were for 2 h. We used the IC-100^{TM} HTM system equipped with CytoShop software^{TM} and customizable with built-in algorithms for the analyses described above. Response curves correlating the efficiency of nuclear translocation (FLIN) of AR-WT and ARC619Y after administration of ligand (Fig. 4) identified the EC_{50} values, and showed that nuclear translocation occurred more efficiently in response to R1881 than OHF, Cas, and E2 (EC_{50} of R1881: 0.03 nM for AR-WT and 0.08 nM for ARC619Y, E2: 0.28 nM for AR-WT and 0.67 nM for AR-619, Cas: 0.58 nM for AR-WT and 1.20 nM for AR619, OHF: 0.86 nM for AR-WT and 1.14 nM for AR-619). R1881 exhibited the best ability to form hyperspeckled intranuclear foci (NVAR), with moderate reorganization from high levels of E2 (10^{-6}M), and this occurred more efficiently with WTAR than with AR619 (Fig. 5a).

To quantify ligand-induced formation of foci for GFP-ARC619Y, an algorithm to measure size and number of cytoplasmic versus nuclear 'vesicles' (e.g., foci in Figs. 2 and 3) was used and show ARC619Y exhibited agonist-dependent foci formation. The EC_{50} value of R1881 for Fractional Localized Intensity in the Vesicle (FLIVSUM)] was 0.50 (Fig. 5b). With the same threshold parameters for the antagonists, no intranuclear foci (FLIVSUM) were measurable (data not shown).

Ligand Dependent AR Mobility

We next performed FRAP analysis to test the effect of ligands on GFP-AR mobility. FRAP showed agonist bound GFP-AR was much less mobile than unliganded receptor in both the cytoplasmic and nuclear compartments (Fig. 6A). In these confocal images, the resolution is decreased due to the rapid scanning (0.2 s intervals) that is required to accurately assess mobility. In untreated cells, bleaching half of the nuclear area lead to decrease in the total fluorescence with the formation of a poorly defined and transient bleach zone. The bleached area recovered rapidly and reached half-maximal recovery ($t_{½}$) in 2.77 ± 0.18 s ($n = 15$) (Fig. 6A,C,D). In contrast, after R1881 treatment, bleaching resulted in a clearly defined zone lacking fluorescence. The fluorescence in the bleach zone rapidly recovered with a half-life ($t_{½}$) of 5.41 ± 0.43 s ($n = 15$) (Fig. 6A,C,D). Treating cells with two different levels of E2 (1 nM and 1 mM) revealed E2 is able to decrease AR nuclear mobility only at higher concentrations (2.6 ± 0.23 s, 3.6 ± 0.27 s, $n = 15$ cells each) supporting E2 as a weak AR agonist at high concentrations (Fig. 6A,C). The recovery half-lives of GFP-AR after Cas and OHF treatments were less than full agonist (R1881) at 2.51 ± 0.16 s, 3.7 ± 0.36 s ($n = 15$ cells each), respectively (Fig. 6B,C).

The mobilities that we report here are significantly different than those reported by Rivera et al. [2003] who reported $t_{1/2}$ times of $\sim$12 s for the agonist-bound GFP-AR and $\sim$7 s for the Cas bound GFP-AR, although our data agree concerning the faster mobility with Cas compared to R1881; however, in general our observations

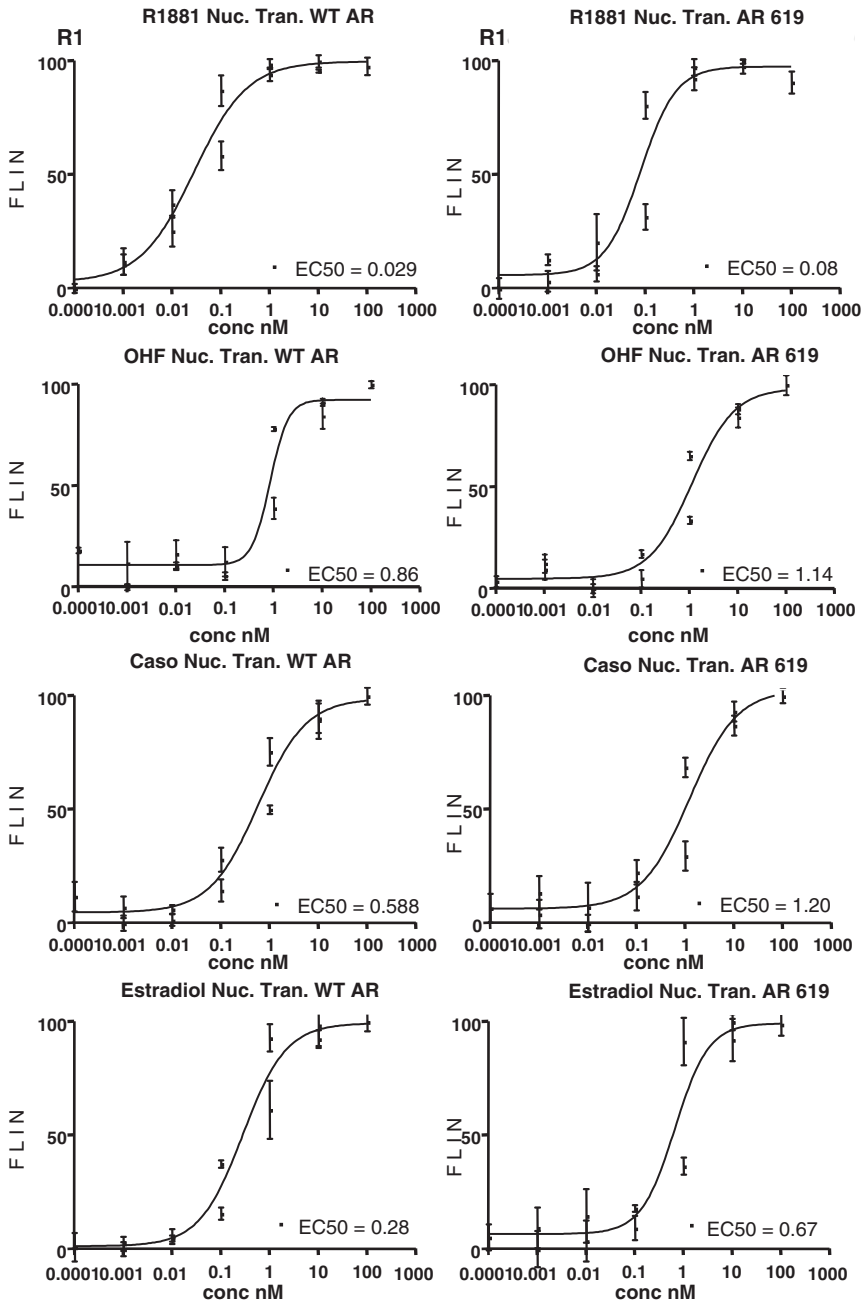

Fig. 4. Quantifying ligand and mutation-dependent subcellular trafficking of AR using high throughput microscopy. Using an 11-point dose response approach over 2 h (in triplicate) and a 96-well approach, we utilized autofocusing, high resolution (40× Planapocromat, 0.95 N.A.) imaging system (IC-100, Beckman Coulter) to automatically acquire images of thousands of transiently transfected HeLa cells GFP-AR's. CytoShop™ software (Beckman Coulter) was utilized to quantify nuclear translocation [Fractional Localized Intensity in the Nucleus (FLIN)]. Both wild type and mutant GFP-AR are quantitatively translocated with all ligands, but at different rates, with R1881 inducing movement at much lower hormone levels. Interestingly, OHF has a very sharp versus gradual dose response.

indicate a significantly more mobile AR pool. In our previous FRAP studies on GFP-ER [Stenoien et al., 2001b], we observed that protein overexpression can significantly affect mobility. The FRAP data shown in Figure 6 was taken from cells expressing low levels of GFP-AR. To put this into context of endogenous protein expression levels, we directly compared

GFP-AR levels in our transiently transfected cells with endogenous AR levels in LNCaP cells using quantitative anti-AR immunofluorescence. Shown are images of untransfected LNCaP cells (Fig. 7A) and GFP-AR transfected HeLa cells (Fig. 7B) taken at the same exposure settings for GFP (left panels shown in green) and anti-AR (right panels shown in red). In the transfected HeLa cells, GFP-AR expression levels vary so that overexpressing cells are overexposed in both the green and red channels. Arrows in Figure 7B point to cells that we consider to be low expressing and contain roughly equivalent levels of AR as LNCaP cells. The same field shown in Figure 5B was taken at adjusted exposure settings to show both medium (Fig. 7C, arrows) and high (Fig. 7D, arrow) expressing cells. Notice that in cells expressing

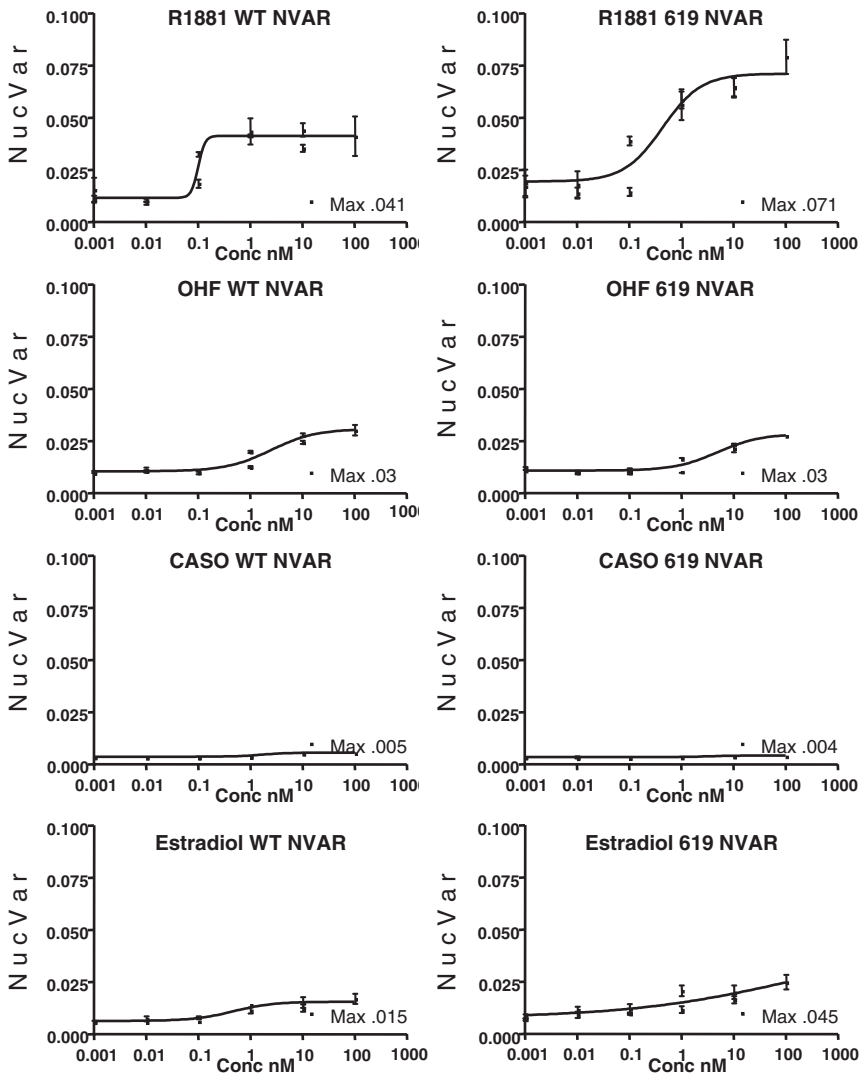

Fig. 5. **a**: Quantifying ligand and mutation-dependent sub-nuclear distribution of wild type and mutant AR using high throughput microscopy. In the same 96-well plates, we calculated the variation in nuclear fluorescence intensity (NVAR). Considering only the coefficient of variation of fluorescence intensity within the DAPI-masked nucleus, data are plotted over the dose response ranges. R1881 shows an early (low concentration) and sharp rise towards a ''hyperspeckled'' organization for wild type GFP-AR. Reflecting both hyperspeckling and foci formation, R1881 leads to a more gradual by marked increase in NVAR for GFP-ARC619Y. Minor increases with higher concentrations of E2 and OHF are also seen. Cas fails to result in nuclear ''hyperspeckeling.'' **b**: Quantifying agonist-induced formation of intracellular foci of GFP-ARC619Y using high throughput microscopy. Also in the same 96-well plates, using an algorithm to detect Fractional Localized Intensity in the Vesicle (FLIVSUM), where R1881-induced GFP-ARC619Y foci are measured as ''vesicles.'' With threshold gating set to specifically define sub-nuclear foci, a marked agonist-induced dose response is observed for GFP-ARC619Y. Other ligands (or wild type AR) completely fail to have defined foci formation when examined using the same algorithm and gating (not shown).

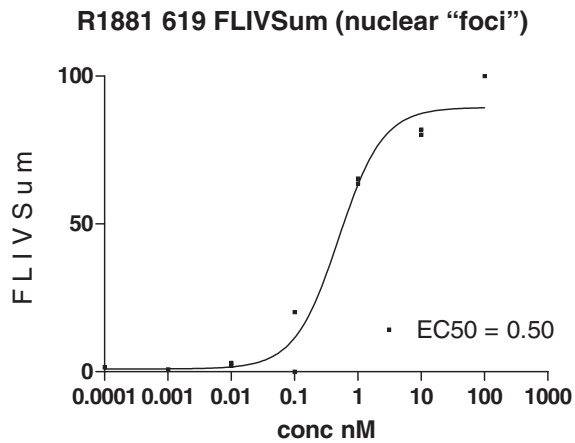

Fig. 5. (*Continued*)

high levels of GFP-AR, peri-nuclear localization in the region of the centrosome is present. As peri-nuclear staining is evident in some published GFP-AR images from other groups [Tyagi et al., 2000; Saitoh et al., 2002; Rivera et al., 2003], differences in expression levels may underscore some of the differences in our results.

To determine the effect of GFP-AR expression levels on mobility, FRAP was performed on cells expressing different levels of GFP-AR. When FRAP was performed on cells expressing low, medium, high and very high levels of AR, a noticeable decrease in GFP-AR mobility was observed at higher expression levels (Fig. 8A). The calculated $t_{1/2}$ times for low, medium, high, and very high expressing cells are 5.2 ± 0.8, 11.4 ± 0.11, 12.1 ± 0.21, and 26.0 ± 3.3, respectively (Fig. 8B; $n = 10$ cells each). Surprisingly, GFP-AR expression levels had little effect on mobility when cells were exposed to either Cas or OHF (data not shown).

Ligand Dependent Change in Solubility of AR

As reported previously, there is a strong correlation between nuclear hyperspeckle formation and nuclear matrix association of the estrogen receptor [Stenoien et al., 2000]. Our experience with detergent extractions and NM preparations on transiently transfected estrogen receptors suggest that overexpression in a sub-population of the cells can skew interpretation of NM association by Western blotting analysis. This has led to conflicting interpretations on the extent of NM association in the presence of ligand for ER ([Htun et al., 1999] vs. [Stenoien et al., 2000] and possibly AR [Tyagi et al., 2000] vs. this study). In order to unambiguously assess the solubility of GFP-AR, we utilized a real-time imaging procedure that allows us to monitor the GFP-tagged proteins in individual cells during the extraction procedure [Stenoien et al., 2000]. Transfected HeLa cells were treated for 2 h with vehicle, R1881, Cas, or OHF at the concentrations used above. The cells were then subjected to a short extraction (3 min) in CSK buffer containing 0.5% Triton X-100. Shown in Figure 9 are the same cells imaged before and after detergent extraction without changing exposure. In all cases, cells expressing low levels of GFP-AR were analyzed to prevent monitoring changes in solubility that is due to overexpression. In the absence of ligand, no detectable fluorescence is retained (data not shown). Cells treated with the agonist R1881 (Fig. 9A) that show a hyperspeckled nuclear distribution of GFP-AR, partially retain the fluorescence after detergent exposure. However, following treatments with Cas (Fig. 9B) or OHF (Fig. 9C), fluorescence is completely undetectable after detergent exposure. These data suggest that detergent-resistance coincides with the discrete sub-nuclear organization and that the hyperspeckled distribution of AR may be a consequence of interactions with nuclear structure. As an example of the effect of overexpression on protein solubility, and in contrast to bulk population-averaged immunoblot data from transiently transfected cell populations (18), we included an overexpressed cell treated with Cas that exhibits strong resistance to detergent extraction (Fig. 9D).

Effect of Ligand on AR and CBP Interactions

Co-activators such as CBP interact with AR and enhance its transcriptional activity. In order to analyze the effects of AR and AR ligands upon co-activator distribution, we performed activity assays and co-localization studies in HeLa cells transiently co-transfected with cyan fluorescent protein-AR (CFP-AR) and yellow fluorescent protein-CBP [YFP-CBP; [Tomura et al., 2001]]. YFP-CBP enhances agonist induced transcription of fluorescently tagged AR approximately 20-fold demonstrating that is retains its co-activation function (Fig. 10A). Following agonist addition, CFP-AR and YFP-CBP co-localize in the same nuclear foci suggestive of some degree of interaction albeit it is very likely at a transient level per the

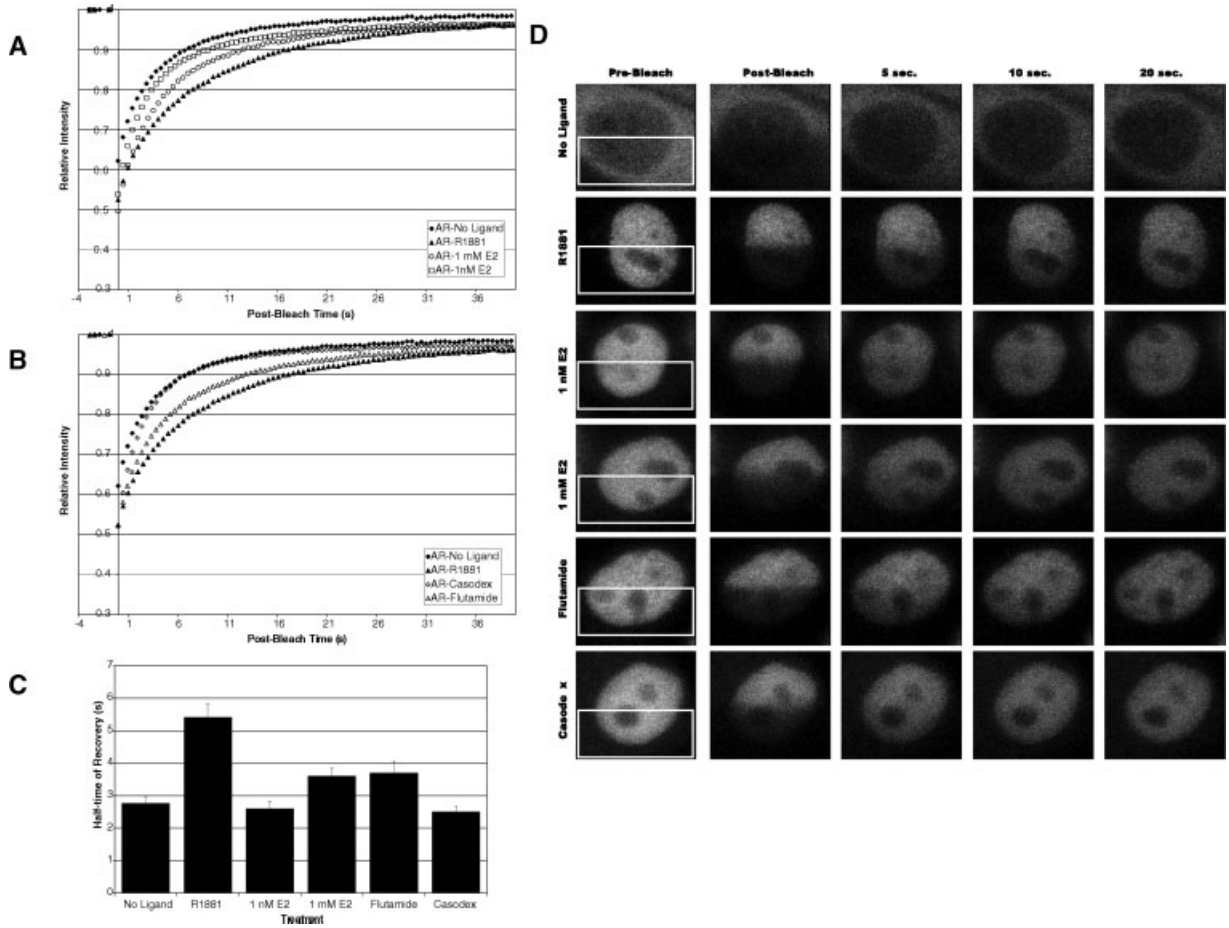

Fig. 6. FRAP of GFP-AR. GFP-AR dynamics in transfected HeLa cells were analyzed through a photobleaching approach after 2 h of hormone treatment. **A**: Graph comparing recovery dynamics in the absence of ligand (◆) and in the presence of 10 nM R1881 (▲), 1 nM E2 (□), and 10 nM E2 (○). Both R1881 and 10 nM E2 treatment are able to reduce the mobility of AR within the nucleus. **B**: Graph comparing the recovery dynamics in the absence of ligand ((◆) and in the presence of 10 nM R1881 (▲), 1 μM Cas (◇), and 1 μM OHF (△). Cas bound AR remains highly mobile within the nucleus, whereas OHU bound AR shows partial reduction in mobility. **C**: Bar graph representing calculated recovery half-time ($T_{1/2}$). R1881 results in the longest recovery time; 10 nM E2, and OHF treatment result in a significant, but much less (~50%) increased $T_{1/2}$. Cas and 1 nM E2 treatment do not significantly change recovery times. **D**: Selected images from half-FRAP experiments.

FRAP data (Fig. 10B,C). To further analyze the interaction between AR and CBP, we performed dual FRAP in HeLa cells co-transfected with CFP-AR and YFP-CBP (Fig. 10D). In the absence of hormone, both CFP-AR and YFP-CBP remain highly mobile (data not shown). After treatment with the agonist R1881, AR shows the same recovery dynamics as in the single transfection above; moreover, CBP and AR recovery parallel each other suggesting agonist addition induces (presumably direct) interactions that can slow CBP mobility. In the presence of Cas (and the other antagonists above, not shown), YFP-CBP remains highly mobile as shown in Figure 10E. While the nature and function of agonist-induced foci remain unclear, the mobility data suggests AR-CBP "complexes" are much less stable in the living cell than in vitro approaches using lysed cells. A large survey of nuclear proteins by Phair et al. recently indicated most chromatin associated proteins are highly dynamic and suggest stochastic movement and interactions play an important role in their function (e.g., scanning the genome).

DISCUSSION

The use of GFP (or its spectral variants, CFP/YFP) tagged steroid receptors allows for real-time imaging to determine the dynamic events that occur following ligand exposure. Studies on

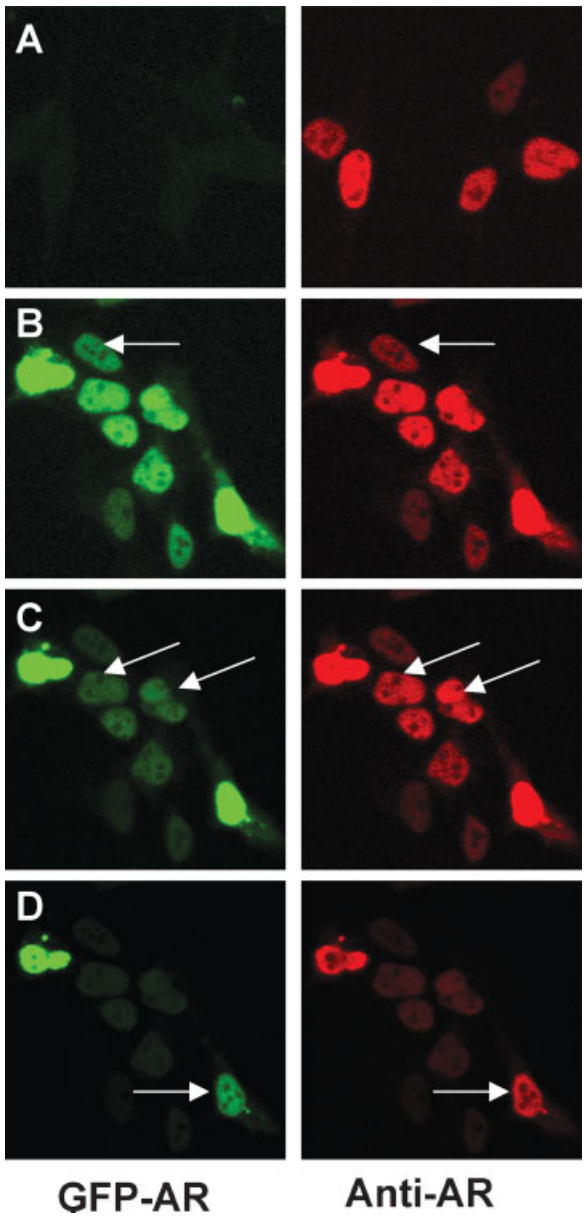

Fig. 7. Relative AR levels in LNCaP and transfected HeLa Cells. LNCaP cells (**A**) and HeLa cells transfected with GFP-AR (**B–D**) were probed with an anti-AR antibody to determine the relationship between GFP-AR and endogenous AR levels. The images in A and B were acquired at the same exposure levels. In the transfected HeLa cells, GFP-AR expression varied so that some cells contain much higher protein levels (and, therefore, are overexposed) than found in cells that naturally express AR. Arrows in B point to cells that were considered low expressing with GFP-AR levels close to endogenous levels. (This level of expression is used for all imaging unless otherwise stated). The exposure levels were reduced to show medium (C arrows) and high (D arrow) expressing cells. Notice that in many cells expressing high GFP-AR levels, there is an accumulation of GFP-AR at the centrosomal region.

GFP-tagged ER [Htun et al., 1999; Stenoien et al., 2000] have shown that agonist addition resulted in a rapid (10–20 min) reorganization of the diffuse ER into distinct intranuclear foci. In the case of AR, agonist addition resulted in a major translocation of the receptor from the cytoplasm to the nucleus where it becomes organized into unstable foci that are even more hyperspeckled than agonist-bound ER foci. Interestingly, AR antagonists also caused nuclear translocation but without the accompanying focal distribution indicating that these are distinct and separate events. Furthermore, the antagonist-bound AR behaved similarly to unliganded ER in terms of its distribution, solubility, and mobility [Stenoien et al., 2000, 2001b], for example, highly diffuse, completely soluble, and more mobile.

Acquiring statistically relevant data at the single cell level is extremely laborious and often operator-dependent. For this reason we applied the relatively new concept of HTM to obtain curves summarizing observations from hundreds of cells with regards to the sub-cellular localization of wild type AR and ARC619Y after stimulation with a variety of ligands given at different concentrations. The results confirmed that a quintessential AR agonist, R1881, is the more efficient ligand in inducing AR nuclear translocation and formation of hyperspeckled foci. While the pattern observed with the two antagonists was essentially similar to what described in low throughput microscopy [i.e., less efficient nuclear translocation by a factor of 20 (Cas) and 30 (OHF) and lack of hyperspeckled nuclear foci]. E2 was about 10-fold less efficient than R1881 in promoting nuclear translocation, and unable to induce formation of hyperspeckled intranuclear foci, except at supraphysiological doses consistent with a weak agonist activity.

Interestingly, the HTM approach also allowed a quantitative means to evaluate the sub-cellular response of AR619 to the ligand panel, and underscores the ligand and dose dependent effects are distinct between wild type AR and this prostate cancer-associated mutant. Overall HTM is an extremely powerful new technology, which holds great promise in single cell analysis, including improving image segmentation, simple feature extraction (distinguishing subtle changes in 'hyperspeckling' from 'foci' formation, artifact rejection (eliminating overexpressers from analyses), and drug

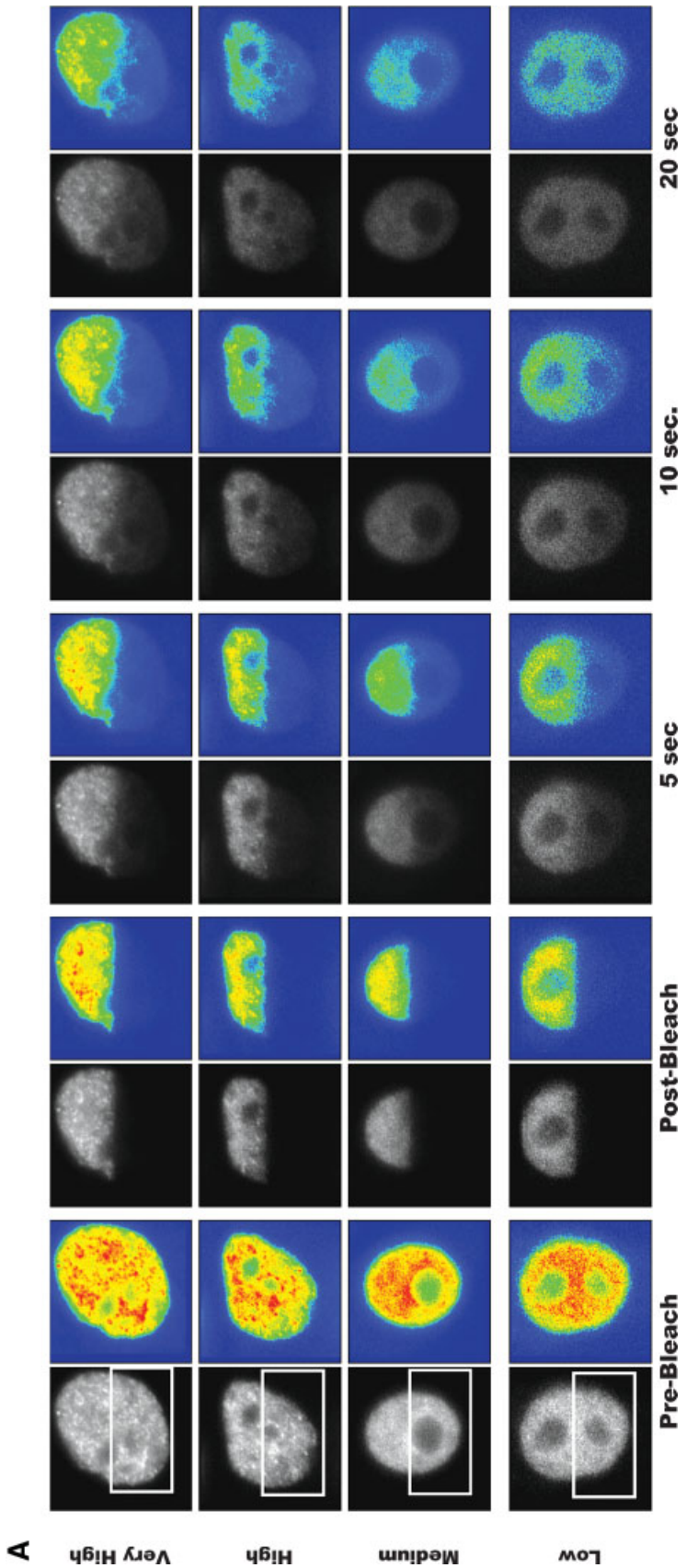

Fig. 8. Expression levels affect GFP-AR mobility. To determine the effect of GFP-AR expression levels on mobility, FRAP was performed on cells expressing different levels of GFP-AR. **A**: When FRAP was performed on cells expressing low, medium, high, and very high levels of AR, a noticeable decrease in GFP-AR mobility was observed at higher expression levels. **B**: The calculated t1/2 times for low, medium, high and very high expressing cells are 5.2 ± 0.8, 11.4 ± 0.11, 12.1 ± 0.21, and 26.0 ± 3.3, respectively ($n = 10$ cells each).

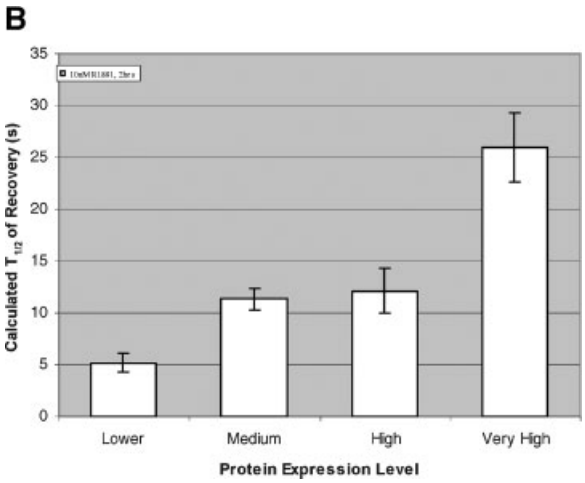

Fig. 8. (*Continued*)

discovery based upon morphological criteria. For example, a drug screen looking for degree of nuclear translocation (FLIN) and sub-nuclear distribution (NVAR) could be data-mined simultaneously with effects on chaperone-binding to AR (geldanamycin data, Fig. 3C,D), and protein folding (foci formation). Further, high throughput multiplexing with an AR dependent promoter driving expression of a fluorescent protein reporter is in progress, to directly relate the subcellular movements and organization with transcriptional reporter activity (A Szatran et al., in prepration).

Since much of the protein machinery for transcription, RNA splicing, and DNA replication is found associated with the NM, this structure may provide a framework for the organization of nuclear metabolism [Nickerson et al., 1995]. In the case of transcription factors such as steroid receptors, there is a correlation between reorganization and transcriptional competence [Stenoien et al., 2000], however, the functional significance of foci formation remains unclear. This uncertainty is due to the observation that few transcription factor foci co-localize with active, focal sites of transcription [Stenoien et al., 2000], and, also that some receptors do not reorganize in response to ligand [Dong et al., 2004], including a deletion mutant of AR that lacks the entire LBD [Farla et al., 2004].

A potential explanation for this observation is that interactions between transcription factors and transcription sites are far more transient than previously thought. The non-localizing transcription factor foci may be in the process

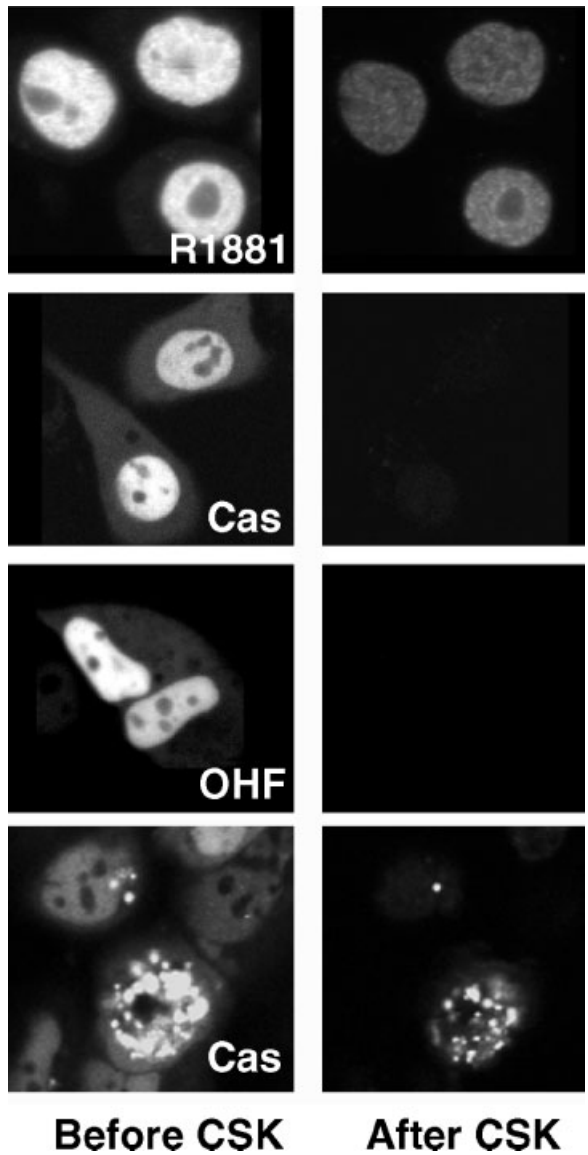

Fig. 9. GFP-AR exhibits differential solubility in the presence of ligands After 2 h of treatment with vehicle or ligands, the same cells were imaged before (left panel) and after extraction (right panel) in CSK buffer containing Triton X-100 detergent for~3 min. In the absence of hormone, most of the cytoplasmic GFP-AR fluorescence is lost. R1881 (5×10^{-9} M) and, to a lesser extent, E2 (10^{-6} M), make GFP-AR partially resistant to detergent extraction. Low concentrations of E2 (10^{-8} M) and the antagonists Cas (10^{-6} M) and OHF (10^{-6} M) fail to induce detergent resistance under normal expression conditions. In cells that overexpress GFP-AR (**D**), some of the GFP-AR fluorescence is retained irrespective of the ligand used.

of development or may have just ended transactivation. In support of this explanation, McNally et al. [2000] used a FRAP approach to demonstrate that glucocorticoid receptors undergo rapid exchange with their DNA target

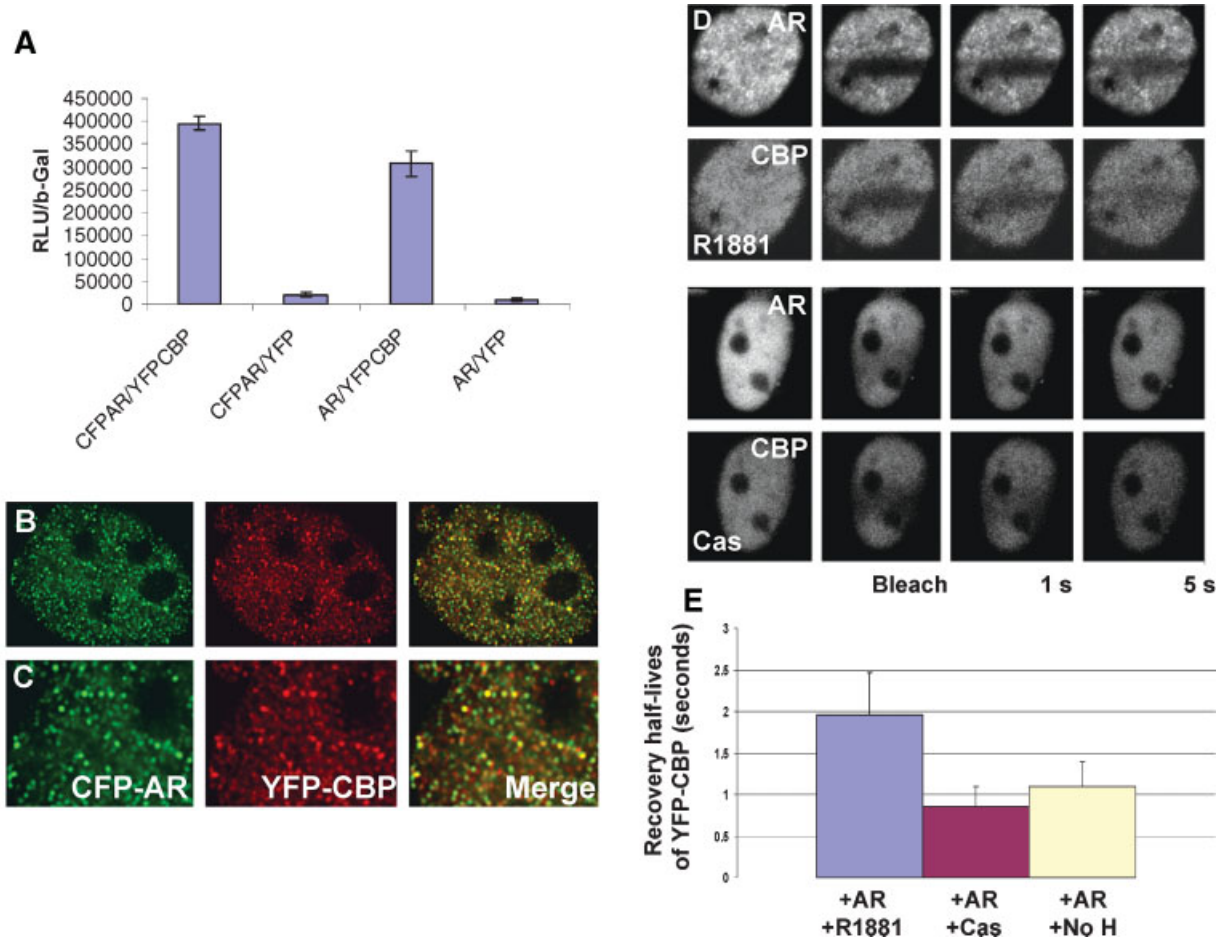

Fig. 10. YFP-CBP retains co-activator activity and co-localizes with R1881 induced CFP-AR foci. **A**: Transactivation assays were performed in the presence of R1881 on HeLa cells co-transfected with CFP-AR and YFP-CBP, CFP-AR and YFP, AR and YFP-CBP, or AR and YFP, and a GRE-Luc reporter plasmid. YFP-CBP significantly enhances CFP-AR and AR activity compared to the YFP control vector alone indicating that it retains its co-activator activity. **B**: HeLa cells were co-transfected with CFP-AR (shown in green) and YFP-CBP (shown in red) and treated for 1 h prior to fixation. **C**: The same cell is shown at higher magnification to show regions of overlap between CFP-AR and YFP-CBP more clearly. **D**: Dual FRAP of CFP-AR and YFP-CBP. HeLa cells were co-transfected with CFP-AR and YFP-CBP and subjected to FRAP analysis of both the CFP-AR (top row) and YFP-CBP (bottom row). In the presence of R1881 (5×10^{-9} M, 1 h), CFP-AR and YFP-CBP show parallel recovery times. In the presence of Cas and other antagonists (data not shown), no reduction in CFP-AR or YFP-CBP mobility is observed. **E**: The recovery half-lives of YFP-CBP under various conditions are shown.

sites. Further, Phair et al report in a comprehensive study on the mobility of chromatin associated proteins that the nucleus is likely more stochastic than expected from biochemical studies alone [Phair et al., 2004].

With GFP-AR, we observed two basic extremes in mobility rates for the agonist ($t_{½}$~5.5s) and antagonist ($t_{½}$~2.5 s) bound receptors. Our FRAP experiments on nuclear GFP-ER also demonstrated that steroid receptors can exhibit different types of intranuclear mobility dependent upon their ligand-bound state [Stenoien et al., 2001b]. GFP-ER mobility ranged from rapid in the absence of ligand ($t_{½} = \sim 0.8$ s) to very slow (little recovery over many minutes) in the presence of the pure antagonist, ICI 182,780. In the presence of agonist, GFP-ER remained mobile but was slowed compared to the absence of ligand ($t_{½} = \sim 5$ s). The agonist-bound GFP-AR exhibited mobility more similar to agonist-bound GFP-ER, while antagonist-bound GFP-AR exhibited the rapid mobility seen with unliganded-GFP-ER, although OHUF had moderately slowed mobility. In our limited survey of AR antagonists, none yet have been shown to immobilize the receptor at physiological expression levels, suggesting that the ER and AR

antagonists that have been tested function through different mechanisms in terms of their effects on receptor mobility.

As steroid receptors have been reported to associate with steroid receptor co-activators in an agonist dependent manner (Reviewed in [McKenna et al., 1999]), we used YFP-CBP to study its dynamics in relation to CFP-AR. In the absence of hormone, negligible overlap was observed between CFP-AR and YFP-CBP (not shown). Addition of R1881 resulted in a substantial overlap between the YFP-CBP and CFP-AR in foci suggesting sub-nuclear regions for interaction, if not an in vivo correlate of a biochemically-defined "complex." FRAP studies confirmed these findings: YFP-CBP mobility was slowed only in the presence of CFP-AR plus agonist. However, it is appropriate from these studies that the notion of 'complex formation' should be considered in the context of living cells: the receptor–co-activator stability in vivo appears to be substantially less than implied by biochemical approaches. In the presence of antagonists, it is difficult to conclude if interactions exist due to the diffuse distribution of YFP-CBP and CFP-AR throughout the nucleus. However, the lack of immobilization seen in FRAP studies which include AR and antagonists suggests that complex formation is minimal, and would even be less stable than those induced by agonist. We reported similar results for fluorescently tagged ER and SRC-1 that show agonist facilitates ER/co-activator interactions [Stenoien et al., 2000, 2001b] and that antagonists may actually inhibit interactions [Stenoien et al., 2001a].

Our laboratory has utilized several approaches to study interactions with the NM that include classical NM preps on fixed cells, and our newly developed protocol to follow extractability starting with single live cells. This method involves analyzing individual cells before, during, and after the extraction protocol to obtain an unambiguous assessment of the extent of NM association of fluorescently-tagged proteins. An important finding from these real-time analyses is that protein expression levels can affect the extent of NM association, as they do for FRAP studies. In cells where ER or AR is overexpressed, the receptors become largely insoluble regardless of their ligand bound state, whereas in cells that express lower levels of protein, receptor solubility is greatly influenced by ligand [Stenoien et al., 2000]. Quantitative approaches suggest a relatively high tolerance of the nucleus to increased expression of specific proteins more than other, with mobility changes noted for ER only when approximately 100-fold over endogenous levels, and the pituitary transcription factor Pit-1 only with inactivating point mutations [Stenoien et al., 2001b; Sharp et al., 2004]. When the solubility of transfected proteins is analyzed by western blotting techniques, the results can be skewed by the presence of the small number of cells that overexpression large amounts of protein. This may be a potential explanation for why our results differ from those of Tyagi et al. [2000] who used a Western blot-based approach to analyze the solubility of transiently transfected AR. Indeed, our single cell studies of Pit-1 mutants also revealed their tight NM association reported originally [Mancini et al., 1999] was greatly affected by overexpression [Sharp et al., 2004].

Single cell analysis of live cells during hormone addition shed light on the rapid changes in AR function that result in nuclear translocation and a reduction in intranuclear mobility. Similar to ER, when compared to unliganded AR, agonist addition results in the formation of intranuclear AR foci that bind to nuclear structure and exhibit reduced mobility. These findings suggest that activated forms of some steroid receptors must become at least dynamically associated with foci prior to transcription, and remain dynamic even at promoters [McNally et al., 2000]. However, as transcription factor foci only partially overlap (and at best very briefly) with sites of transcription, additional regulator issues involving sub-nuclear navigation of key factors must exist and remain an exciting area of future research.

ACKNOWLEDGMENTS

The authors thank Maureen Mancini and Kavita Patel for excellent technical assistance. This work was funded by DK 55622 (M.A.M.). The imaging studies were performed in the Integrated Microscopy Core, funded in part by NIDDK sponsored Center for Reproductive Biology (U54 HD-96-008), and additional support from Prostate Spore grant CA58204.

REFERENCES

Czar MJ, Galigniana MD, Silverstein AM, Pratt WB. 1997. Geldanamycin, a heat shock protein 90-binding

benzoquinone ansamycin, inhibits steroid-dependent translocation of the glucocorticoid receptor from the cytoplasm to the nucleus. Biochemistry 36:7776–7785.

Dong S, Stenoien DL, Qiu J, Mancini MA, Tweardy DJ. 2004. Reduced intranuclear mobility of APL fusion proteins accompanies their mislocalization and results in sequestration and decreased mobility of retinoid X receptor alpha. Mol Cell Biol 24:4465–4475.

Farla P, Hersmus R, Geverts B, Mari PO, Nigg AL, Dubbink HJ, Trapman J, Houtsmuller AB. 2004. The androgen receptor ligand-binding domain stabilizes DNA binding in living cells. J Struct Biol 147: 50–61.

Fejes-Toth G, Pearce D, Naray-Fejes-Toth A. 1998. Subcellular localization of mineralocorticoid receptors in living cells: effects of receptor agonists and antagonists. Proc Natl Acad Sci USA 95:2973–2978.

Feldman BJ, Feldman D. 2001. The development of androgen-independent prostate cancer. Nat Rev Cancer 1:34–45.

Georget V, Lobaccaro JM, Terouanne B, Mangeat P, Nicolas JC, Sultan C. 1997. Trafficking of the androgen receptor in living cells with fused green fluorescent protein-androgen receptor. Mol Cell Endocrinol 129: 17–26.

Htun H, Holth LT, Walker D, Davie JR, Hager GL. 1999. Direct visualization of the human estrogen receptor alpha reveals a role for ligand in the nuclear distribution of the receptor. Mol Biol Cell 10:471–486.

Jemal A, Tiwari RC, Murray T, Ghafoor A, Samuels A, Ward E, Feuer EJ, Thun MJ. 2004. Cancer statistics, 2004. CA Cancer J Clin 54:8–29.

Jenster G, Trapman J, Brinkmann AO. 1993. Nuclear import of the human androgen receptor. Biochem J 293: 761–768.

King WJ, Greene GL. 1984. Monoclonal antibodies localize oestrogen receptor in the nuclei of target cells. Nature 307:745–747.

Kopito RR. 2000. Aggresomes, inclusion bodies and protein aggregation. Trends Cell Biol 10:524–530.

Lamb DJ, Weigel NL, Marcelli M. 2001. Androgen receptors and their biology. Vitamines and Hormones 62:199–230.

Mancini MG, Liu B, Sharp ZD, Mancini MA. 1999. Subnuclear partitioning and functional regulation of the Pit-1 transcription factor. J Cell Biochem 72:322–338.

Mangelsdorf DJ, Thummel C, Beato M, Herrlich P, Schutz G, Umesono K, Blumberg B, Kastner P, Mark M, Chambon P, et al. 1995. The nuclear receptor superfamily: the second decade. Cell 83:835–839.

Marcelli M, Ittmann M, Mariani M, Sutherland R, Nigam R, Murthy L, Zhou Y, DiConcini D, Puxeddu E, Esen A, Eastham J, Weigel NL, Lamb DJ. 2000. Androgen receptor mutations in prostate cancer. Can Res 60:944–949.

McKenna NJ, Lanz RB, O'Malley BW. 1999. Nuclear receptor coregulators: cellular and molecular biology. Endocr Rev 20:321–344.

McNally JG, Muller WG, Walker D, Wolford R, Hager GL. 2000. The glucocorticoid receptor: rapid exchange with regulatory sites in living cells. Science 287:1262–1265.

Nazareth LV, Stenoien DL, Bingman WE 3rd, James AJ, Wu C, Zhang Y, Edwards DP, Mancini M, Marcelli M, Lamb DJ, Weigel NL. 1999. A C619Y mutation in the human androgen receptor causes inactivation and mislocalization of the receptor with concomitant sequestration of SRC-1 (steroid receptor coactivator 1). Mol Endocrinol 13:2065–2075.

Nickerson JA, Blencowe BJ, Penman S. 1995. The architectural organization of nuclear metabolism. Int Rev Cytol 162A:67–123.

Phair RD, Misteli T. 2000. High mobility of proteins in the mammalian cell nucleus. Nature 404:604–609.

Phair RD, Scaffidi P, Elbi C, Vecerova J, Dey A, Ozato K, Brown D, Hager G, Bustin M, Misteli T. 2004. Global Nature of Dynamic Protein-Chromatin Interactions in vivo: Three-dimensional Genome Scanning and Dynamic Interaction Networks of Chromatin Proteins. Mol Cell Biol 24(14):6393–6402.

Reid P, Kantoff P, Oh W. 1999. Antiandrogens in prostate cancer. Invest New Drugs 17:271–284.

Rivera OJ, Song CS, Centonze VE, Lechleiter JD, Chatterjee B, Roy AK. 2003. Role of the Promyelocytic Leukemia Body in the Dynamic Interaction between the Androgen Receptor and Steroid Receptor Coactivator-1 in Living Cells. Mol Endocrinol 17:128–140.

Saitoh M, Takayanagi R, Goto K, Fukamizu A, Tomura A, Yanase T, Nawata H. 2002. The presence of both the amino- and carboxyl-terminal domains in the AR is essential for the completion of a transcriptionally active form with coactivators and intranuclear compartmentalization common to the steroid hormone receptors: a three-dimensional imaging study. Mol Endocrinol 16: 694–706.

Sharp ZD, Stenoien DL, Mancini MG, Ouspenski II, Mancini MA. 2004. Inactivating Pit-1 mutations alter subnuclear dynamics suggesting a protein misfolding and nuclear stress response. J Cell Biochem 92:664–678.

Stenoien D, Sharp ZD, Smith CL, Mancini MA. 1998. Functional subnuclear partitioning of transcription factors. J Cell Biochem 70:213–221.

Stenoien DL, Cummings CJ, Adams HP, Mancini MG, Patel K, DeMartino GN, Marcelli M, Weigel NL, Mancini MA. 1999. Polyglutamine-expanded androgen receptors form aggregates that sequester heat shock proteins, proteasome components and SRC-1, and are suppressed by the HDJ-2 chaperone. Hum Mol Genet 8:731–741.

Stenoien DL, Mancini MG, Patel K, Allegretto EA, Smith CL, Mancini MA. 2000. Subnuclear trafficking of estrogen receptor-alpha and steroid receptor coactivator-1. Mol Endocrinol 14:518–534.

Stenoien DL, Nye AC, Mancini MG, Patel K, Dutertre M, O'Malley BW, Smith CL, Belmont AS, Mancini MA. 2001a. Ligand-mediated assembly and real-time cellular dynamics of estrogen receptor alpha-coactivator complexes in living cells. Mol Cell Biol 21:4404–4412.

Stenoien DL, Patel K, Mancini MG, Dutertre M, Smith CL, O'Malley BW, Mancini MA. 2001b. FRAP reveals that mobility of oestrogen receptor-alpha is ligand- and proteasome-dependent. Nat Cell Biol 3:15–23.

Tomura A, Goto K, Morinaga H, Nomura M, Okabe T, Yanase T, Takayanagi R, Nawata H. 2001. The subnuclear three-dimensional image analysis of androgen receptor fused to green fluorescence protein. J Biol Chem 276:28395–28401.

Tsai MJ, O'Malley BW. 1994. Molecular mechanisms of action of steroid/thyroid receptor superfamily members. Annu Rev Biochem 63:451–486.

Tyagi RK, Lavrovsky Y, Ahn SC, Song CS, Chatterjee B, Roy AK. 2000. Dynamics of intracellular movement and nucleocytoplasmic recycling of the ligand-activated androgen receptor in living cells. Mol Endocrinol 14: 1162–1174.

Welshons WV, Cormier EM, Wolf MF, Williams PO Jr., Jordan VC. 1988. Estrogen receptor distribution in enucleated breast cancer cell lines. Endocrinology 122: 2379–2386.